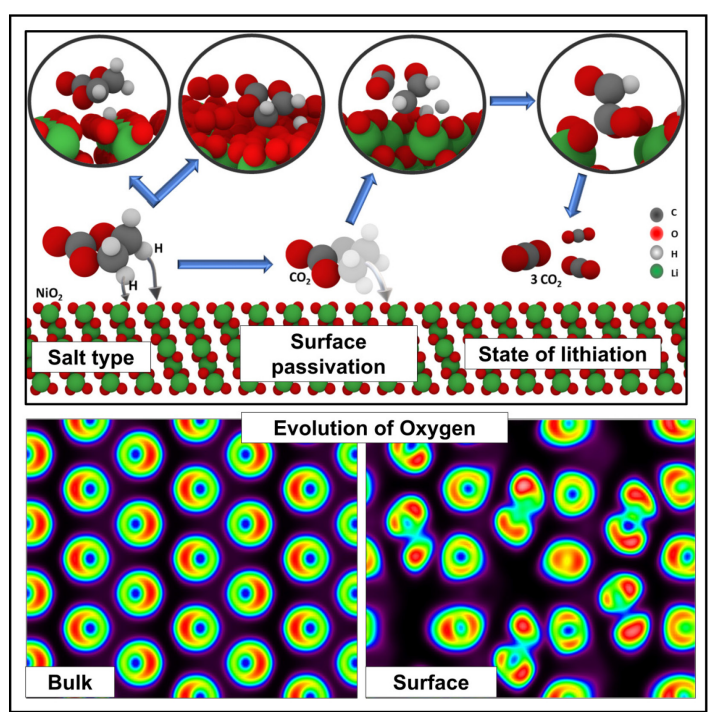
Electrolyte Reactivity, Oxygen States, and Degradation Mechanisms of Nickel-rich Cathodes

M.D. Hashan C. Peiris, ^{1,*} Diana Liepinya, ² Hao Liu, ^{1,3} and Manuel Smeu^{1,4,5,**} ¹Materials Science and Engineering, Binghamton University, Binghamton, NY, 13902, USA ²Materials Science and Engineering, University of Maryland, MD, 20742, USA ³Department of Chemistry, Binghamton University, Binghamton, NY, 13902, USA ⁴Department of Physics, Binghamton University, Binghamton, NY, 13902, USA

*Correspondence: mpeiris1@binghamton.edu



**Correspondence: msmeu@binghamton.edu

Twitter handle: @PeirisMD



SUMMARY

This work explores the interface between fully lithiated/delithiated Ni-rich cathodes and organic electrolytes using density functional theory (DFT) and ab initio molecular dynamics (AIMD). By analyzing the behavior of LiBF $_4$ and LiPF $_6$ salts, we gain valuable insights into atomic-level interactions at the cathode-electrolyte boundary. We observe significantly higher surface activity in delithiated cathodes relative to lithiated cathodes, forming O_2 species in peroxide form, transitioning from a singlet state into a triplet state while being released from the cathode. Ethylene carbonate (EC) dissociation, triggered by surface oxygen radicals, often generates CO_2 and CO on the surface. Variations in Ni and O atomic charges reveal how different lithiation levels affect surface behavior, while the degree of hydrogen passivation significantly influences surface degradation. Lower passivation promotes O_2 evolution, while higher levels lead to O_2 0 formation. These findings highlight the potential of targeted surface modifications to enhance battery performance and safety.

LiNiO₂ Cathode, AIMD, EC/DMC, Li-ion Battery, Cathode-electrolyte interface, Energy storage

INTRODUCTION

Rechargeable lithium-ion batteries (LIBs) are extensively utilized in powering a multitude of items from portable electronic devices to large stationary energy storage systems due to their high storage capacity, long lifetime, electrochemical stability, and reliable performance. However, with the continuous miniaturization of portable electronic devices and driving range limitations in electric vehicles (EVs), demand for new battery chemistries poses interesting challenges for the research community.

A common Li-ion battery configuration consists of a graphite anode, a LiMO₂ cathode where 'M' represents a transition metal in layered oxides (such as LiCoO₂), and an electrolyte formulated from a lithium salt like LiBF₄ or LiPF₆ in a solvent blend of alkyl carbonates (for example, a mix of ethylene carbonate and dimethyl carbonate, abbreviated as EC–DMC). This structure is one of several that have been both studied and commercially applied.^{1,2}

Layered oxides are preferred for cathodes in batteries due to being topotactic (without major alterations in the host structure during cycling), their repeatable reversibility, and moderate change in volume. LiCoO₂ can be deintercalated/re-intercalated reversibly up to a potential of approximately 4.2 V versus Li⁺/Li. It is still the most extensively utilized cathode in Li-ion batteries for a wide range of portable devices owing to its excellent energy density, cyclability, and high-rate capacity^{3,4}. The main drawback of this material is its low reversible capacity, which is restricted to 135 mAh/g when 0.5 Li⁺ is exchanged per mole of Co.^{1,5,6}

Extensive studies have highlighted lithium nickelate (LiNiO₂) and its variants as viable alternatives to conventional LiCoO₂ cathodes due to their structural similarities, cost-effectiveness, and enhanced electrochemical stability during the end stages of charging, thereby reducing electrolyte oxidation⁷. However, achieving a stoichiometric LiNiO₂ composition with an exact Li/Ni ratio of 1 remains a complex synthetic endeavor.⁸ The compound often manifests as Li_{1-z}Ni_{1+z}O₂ (0.2 \geqslant z > 0), a configuration that can compromise its layered structure. This is attributed to the similarity in the radii of Ni²⁺ and Li⁺, resulting in site mixing during synthesis and electrochemical cycling ($r_{Ni(3+)} = 0.56\text{ Å}$, $r_{Ni(2+)} = 0.69\text{ Å}$, $r_{Li(1+)} = 0.76\text{ Å}$).⁸⁻¹⁰

In a battery, the cathode is continually interfaced with the electrolyte, serving as the medium for lithium ion migration to the anode via diffusion processes. Various formulations of organic carbonate-based electrolytes have been extensively studied and are prevalent in commercial battery applications. ^{11–13} Ionic conductivity within the electrolyte is enhanced through the incorporation of lithium-based salts, with Li⁺ serving as the cation. Commercial LIBs predominantly employ inorganic lithium salts (e.g., LiPF₆) dissolved in aprotic polar solvents. Among these, combinations of ethylene carbonate (EC) with other carbonates like dimethyl carbonate (DMC), propylene carbonate (PC), diethyl carbonate (DEC), and ethyl methyl carbonate (EMC) are commonly used, in varying proportions. ¹⁴

Degradation of the battery is complex and often involves a number of interlinked, and interdependent processes. The cathode suffers structural change and degradation, resulting in phase changes, oxidation of lattice oxygen, TM/Li^+ site exchange, and fatigue degradation due to surface reconstruction.^{1,2,15,16} The disparity between theoretical and actual battery capacities is commonly ascribed to electrochemical interactions involving the organic electrolyte, which can result in cathode degradation at elevated voltages.^{1,2} Commonly used electrolytes, such as $LiPF_6$ in a mixture of linear and/or cyclic solvents, are vulnerable to reduction at low voltages near the anode and oxidation near the cathodes at high voltages. There have been a number of investigations into the nature of these processes and are broadly categorized as parasitic and irreversible cathode-electrolyte reactions, trace moisture resulting in the dissolution of transition metals and interactions with electrolyte components, and acidic attack on electrodes by HF generated during the hydrolysis of anions (such as PF_6^-), and reactions between molecules in the bulk electrolyte.² From a more macroscopic standpoint, phase changes during lithium insertion/extraction or thermal effects can cause volume changes in the bulk material. This can result in cracking of the cathodes, while the surface reconstruction during repeated cycling can result in irreversible changes to the structure, hindering Li pathways.^{2,17–21}



Additionally, the kinetic stability of the interface between the electrode and electrolyte is highly reliant on the surface chemistry.¹²

In an ideal battery, cycling should induce no net alteration in the components, with half-cell reactions confined to the electrodes rather than involving the electrolyte.²² For the current work, we were interested in modeling the degradation of two main components of the battery: the cathode surface and the cathode-electrolyte interface. We employ density functional theory (DFT) and *ab initio* molecular dynamics (AIMD) atomistic modeling to study the interactions between bulk electrolyte and the cathode surface using systems which consist of LiNiO₂ cathodes and electrolyte. First, we investigate the dissociation of electrolyte molecules upon contact with the cathode interface at different states of charge (SOC), the effects of salts on interactions, and tendency for the formation of molecular oxygen on various cathode surfaces and SOCs. We calculate the change in charge of the Ni ions in the cathode over time. We also consider the effects of reaction products on the cathode surface from our AIMD results and other works so as to model systems that are farther evolved in time.

RESULTS & DISCUSSION

The primary cathode-electrolyte systems considered for this study are shown in Fig. 1. In addition to these systems, we also consider the surface passivation level of the cathode surface (Fig. S1) We start by investigating the process of degradation of the electrode surface throughout the AIMD trajectory, with a particular interest in the reactions involving oxygen atoms within the cathode and the electrolyte. Thereafter, the degradation of the organic electrolyte molecules is discussed, mainly the formation of CO_2 and H_2O molecules, and the signs of formation of the cathode-electrolyte interphase (CEI). Then we track the change in the charge of Ni in the layered cathode as a function of time and the charge of atoms in the electrolyte molecules as they undergo reactions with the cathode surface. The differences in the trajectories calculated with and without the Hubbard correction are also discussed. Finally, the observations from the systems that were used as a method of advancing the timeline of reactions will be discussed.

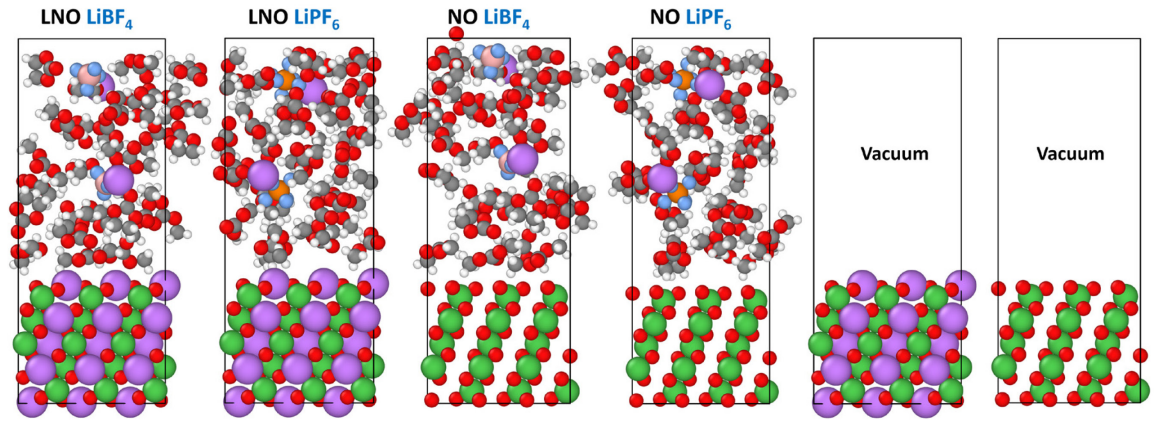


Figure 1. Major systems considered in the study. The four distinct systems with lithiated and de-lithiated Ni-rich cathodes with LiBF₄ and LiPF₆ as salts in the electrolyte and the vacuum cathodes (fully lithiated (left) and fully delithiated (right)). (Legend: Purple-Li, Green-Ni, Red-Oxygen, White-Hydrogen, Grey-Carbon, Orange-P, Pink-Boron, Blue-Fluorine)

Surface reconstructions

Immediate surface reconstruction of the cathode surface was observed for all trajectories except for the pre-passivated surfaces. The reconstruction was mainly by way of protrusion of Li from the bulk lattice sites (Fig. 2(i-ii) and S2/S3). In the delithiated surfaces, reconstruction by way of combination of nearby oxygen atoms into molecular oxygen was more prominent. Lithiated vacuum cathodes displayed behavior akin to those in contact with electrolytes. We further studied the surface reconstruction process using partial and full coverage with hydrogen terminations. Full coverage of the surface mitigated lithium ion protrusion completely, underscoring the role of dangling bond treatment in cathode design, and the study of reactions at the surface. However, when surface passivation was applied to the delithiated cathodes, formation of molecular H_2O was observed more frequently compared to O_2 formation. This passivation dependency on the cathode surface evolution is discussed in detail.

Formation of molecular oxygen

Recent studies have indicated that the formation and reactivity of singlet oxygen at the cathode interface could be a significant factor in the degradation of LiNiO₂ cathodes.^{23–26} This has also been tied to the observation of CO₂ and CO emissions, with a notable presence of singlet oxygen activity. Previous investigations into this phenomenon have employed atomistic simulations



that included interactions between the electrolyte and nickel-rich cathode surfaces, allowing the detection of singlet oxygen in both the presence and absence of electrolyte.²³

It is now understood that the electrolyte component, especially ethylene carbonate (EC), typically does not react with triplet oxygen under normal operating temperatures of Li-ion batteries.^{23,24,26,27} The emergence of CO and CO₂ has been linked to reactions with reactive oxygen species originating from nickel-manganese-cobalt (NMC) cathodes, a hypothesis supported in our simulations for the Ni-rich (012) facets in this work, see *Reaction Pathways - Formation of CO₂*. These show that singlet oxygen and oxygen radicals on the cathode surface promote the dehydrogenation of EC.

Experimental evidence has captured the thermal release of singlet oxygen from delithiated Ni rich cathodes.²⁸ They observed a subsequent surge in electrolyte oxidation products suggesting an electrochemical origin for the singlet oxygen. Previous computational work indicates that despite the Ni maintaining a +2 charge post-delithiation, the Ni–O bond environment undergoes alterations, leading to Jahn-Teller distortions, as corroborated by prior computational studies on the effects of Jahn-Teller distortions, (Li-Ni-vacancy)O phase diagrams and extended X-ray absorption fine structure (EXAFS) analyses.^{10,23,29}

In our simulations, we observed significant protonation at the delithiated cathode surface due to dehydrogenation of EC and DMC (Fig. S2-S3). We also observed the formation of stable H_2O at the cathode surface when the level of protonation was at a level where the hydrogen at the surface would prefer to combine and form molecular H_2O . Experimentally, the presence of water at the cathode interface, especially at higher voltages, is a known aspect of cathode operation in NMCs. $^{2,30-32}$ This has also been shown to result in the introduction of protons and intercalated water into the layered cathode materials and reducing the diffusivity of Li into the layered structure. 30

Our charge analysis of NiO_2 surfaces via both Bader and DDEC6 charge analysis reveals distinct oxidation of surface oxygen atoms at the pristine cathode surface compared to the bulk (Fig. S13). The dynamics of the surface in our trajectories indicate that the (012) NiO_2 surface can spontaneously lose oxygen molecules and form singlet oxygen, as has been seen very recently by other groups [49]. They conclude that the process is seemingly barrier-less with the desorption energy barrier for O_2 release calculated to be about 0.04 eV and is well below the thermal fluctuations.^{23,33} Our simulations confirm this, enabling the desorption of O_2 species from the surface in our trajectories into the electrolyte region in the triplet state (Fig. 2(b)).

Further analysis of the magnetic properties and charge densities at the cathode surface enabled us to elucidate the radical nature of the surface oxygen atoms and the formation of peroxide ions when two radicals come into proximity (Fig. S14). This leads to the creation of a covalent O–O bond, forming a dimer. This dimer formation process is observed on both the (012) facet in our simulations and has been observed for the (104) facet of NiO₂. ³³ For the (104) surface the dimer formation is across the layer, while for the (012) surface the oxygen atoms combine with their immediate neighbors. Given the prevalence of the (012) facet experimentally, the oxygen release from this facet has been explained to be the most representative of the overall behavior of Ni-rich cathodes. ^{23,34}

More specifically, in our trajectories, the formation of O_2 at the cathode surface was only observed in the de-lithiated state and had comparatively higher vertical movement (away from the cathode surface) in the vacuum system compared to the cathodes with electrolyte (Fig. 2(a), by about ~1.75 Å. A tethered motion was observed in the case of both de-lithiated cathodes (with and without the electrolyte present) where most O_2 species that formed, stayed bound to the Ni ion by a single oxygen (Ni- O_1 bond distances in Fig. 2(b) and Fig. S4). This surface-bound species was identified to be the peroxide state of the O_2 anion, using spin density and magnetization (~0 μ B) (Fig. S15). Occasionally, the peroxide species that form on the delithiated cathodes exhibited complete desorption from the surface, resulting in the oxidization of the peroxide ion to a singlet oxygen, briefly, and then on to molecular oxygen at the triplet state (Figs. S14 and S15). Since the conversion time from a peroxide state to triplet state through the singlet state was very short (few hundred femtoseconds in our trajectory), we only captured one instance of an electrolyte molecule fragment (EC) reacting with the singlet species (Fig. S20). The tendency for the formation of 1O_2 species has very recently been theorized to be due to the spin conservation rules favoring the release of singlet state peroxides.²³

The energy required for the desorption of such O₂ molecules from the cathode surface, as defined by Equation 1,

$$E_{desorption} = (E_{cathode} + E_{O_2}) - E_{cathode with O_2},$$
 (1)

was calculated for individual snapshots of the trajectory of delithiated cathode without electrolyte every 500 fs. E_{cathode} is the single point total energy of the system with the isolated cathode, E_{O2} is the energy of the isolated O_2 molecule and E_{cathode} with O_2 is the energy of the total system. The results, as illustrated in Fig. 2(b), show that shortly after the formation of the O_2 molecule, it achieves a negative desorption energy making it energetically favorable for the O_2 molecule to evolve from the surface.

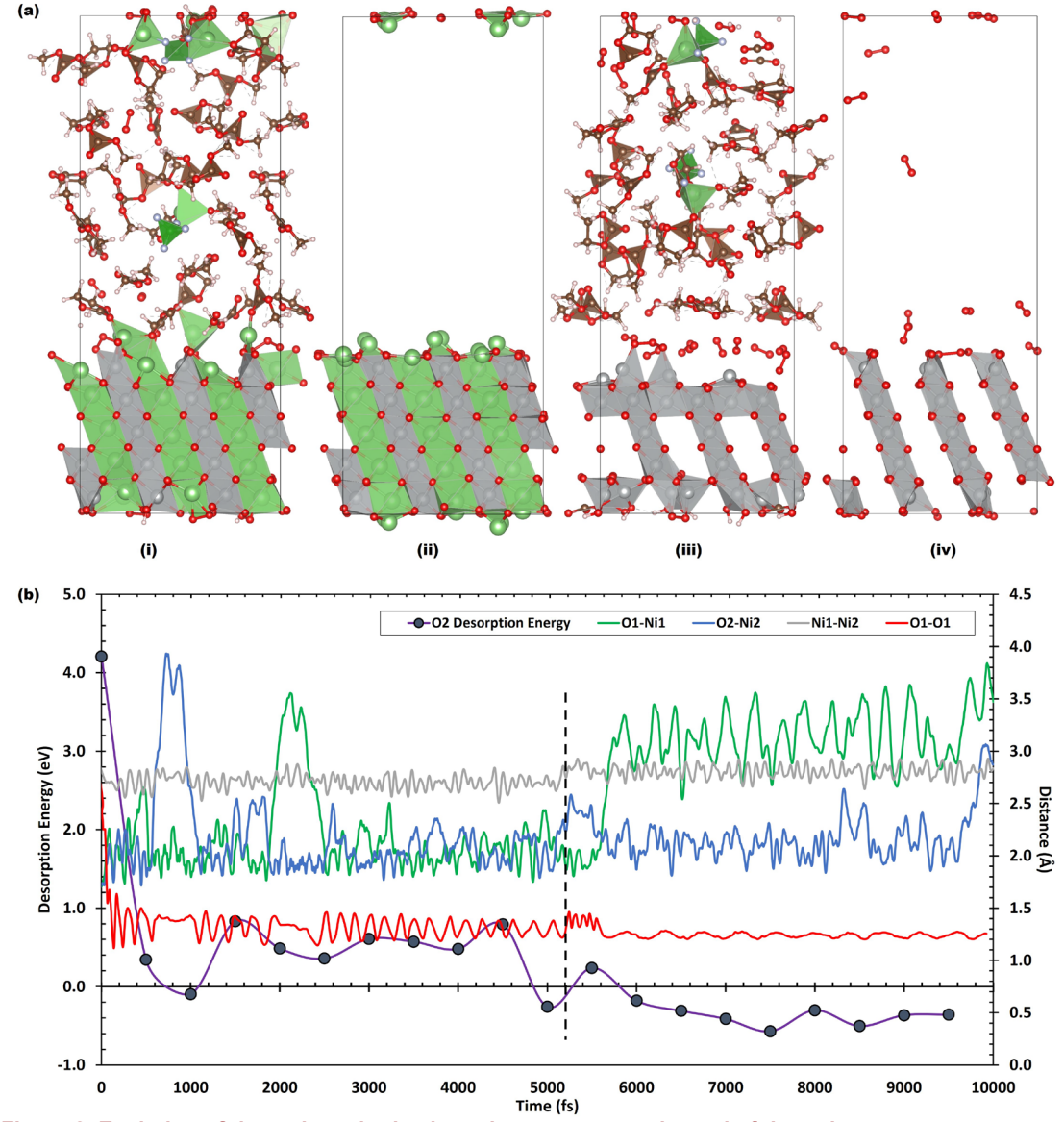


Figure 2. Evolution of the main cathode-electrolyte systems at the end of the trajectory (A) Evolution of the cathode surface for non-passivated lithiated (i-ii) and delithiated (iii-iv) surfaces with and without electrolyte, resulting in a surface reconstruction and O_2 evolution in delithiated cathodes (DFT+U). The sustained heights for O_2 molecules evolving at the cathode surface seen in a(iii) is ~ 3.5 Å. (B) Desorption energies for the surface evolution of an O_2 molecule in a delithiated NiO₂ vacuum cathode, evaluated every 500 fs steps with the variation of the distance between the two individual oxygen atoms (O1-O2), and the respective Ni neighbors in the process (Ni1-O1 and Ni2-O2). The point in time where the O_2 molecule fully evolves from the surface is indicated by the dashed line, resulting in a slight increase in Ni-Ni separation at the site. (Ni-grey, Li-green, O-red, H-white, F-blue, and B contained within the tetrahedrals of F (BF₄ $^-$).



Once the peroxide ion converts to an O_2 molecule, it leaves the surface becoming a triplet oxygen, verified using three methods, namely bond distance, charge analysis (DDEC6) and visualization of ELF. Fig. 2(b) illustrates the change in bond distances of relevant atoms in an instance where O_2 forms on the cathode surface. Here, two nearby oxygen atoms which were originally bound to two Ni atoms combine into an O_2^{2-} peroxide ion, which remains bound to the surface by one of the Ni atoms on the surface. The average oxygen to oxygen bond distance after the formation of the molecule (at ~6250 fs) matched the bond distance of an O_2 molecule (121 pm) (Fig. 2).³⁵ Visualization using ELF iso-surfaces was used as a method of classification of chemical bonds allowing a reliable characterization of covalency versus ionicity to be determined.³⁶ The ELF visualization of variable iso-surfaces of the isolated O_2 molecule referred to in Fig. 2(b) is provided for reference (Fig. S6).

In the absence of external perturbations, the direct transition from an excited singlet state to the triplet ground state in oxygen molecules is highly unlikely due to the strict rules governing electric dipole transitions, which are influenced by the symmetry and spin properties of the molecule's electronic states. This process has not yet been fully investigated in the context of cathode-electrolyte interfaces. However, detailed studies have been carried out to investigate the transition pathways from the singlet to triplet state for both unperturbed and perturbed O_2 molecules in various gas and solvent systems³⁷. Hence, in isolated O_2 molecules, the transitions from singlet to triplet states are primarily governed by radiative deactivation processes.

However, the interaction of O_2 molecules with other atoms or molecules induces perturbations in their electronic structure, which can partially lift the forbidden nature of the transition. Such perturbations enable partially allowed character in radiative transitions and facilitate alternative deactivation pathways. Three major modes enabling such a transition have been found to be from Electronic-to-Vibrational (e-v) Energy transfer, Charge-Transfer Induced Quenching (CT), and Electronic Energy Transfer (EET).³⁷ These processes have been found to be further influenced by the physical properties of the quenching agent and the medium, such as the size of the collider molecules, solvent refractive index, collision frequency, and van der Waals volume. These factors affect the rate constants and the efficiency of the deactivation processes. Additionally, the interactions of O_2 with surfaces, such as in the case of peroxide/ O_2 molecule interaction, has been observed to provide mechanisms for the otherwise spin-forbidden relaxation from singlet to triplet states.²³

There was a discernible difference in the desorption of the O_2 molecules for the trajectories run with the U correction and spin polarization, relative to the trajectories run with no correction for electron correlation. The Hubbard U corrected trajectories permitted complete desorption of the O_2 formed by lattice breakdown in cathode systems modeled with vacuum as well as with electrolyte. Consequently, this resulted in the instability of the lattice, leading to dislodging of Ni atoms. The Ni atoms were then observed to move into inter-layer sites as discussed previously. The O_2 molecules were seen to form on both lithiated and delithiated cathodes (albeit much more prominent on the delithiated surfaces). After the non-reversible evolution of neighboring O_2 , Ni atoms subsequently displaced from their original sites within the stratified lattice structure, stabilizing inside the Li channels (Fig. S7). We identify this as the layered-to-spinel phase change induced at high charge states induced by molecular O_2 formation. It is well known that the DFT calculations on transition metal oxides necessitate accounting for the localized and strongly correlated d electrons. The motivation for trialing the non-U corrected trajectories in this work was to investigate the necessity and implications of U correction for AIMD calculations, given the relative expense of the DFT+U calculations, dearth of literature in the context of AIMD and the difficulties of ionic convergence at these scales of AIMD simulations. Apart from complete desorption of O_2 from the cathode as described above, a few instances of O_3 species, O_3 and a generally more chemically active interface was observed for the trajectories with the U correction enabled. (see Sec. 3.2.2 and Figs. S18 and S19). The observations we made in our trajectories have been observed experimentally. O_3 species and O_3 species are simple trajectories have been observed experimentally.

Based on our simulations with the systems without electrolyte compared to systems with electrolyte, we see no significant differences in the initial reconstruction/degradation mechanisms. Both systems exhibit removal of surface oxygen via the evolution of H_2O and O_2 . The surfaces seem to stabilize after the initial release of O_2 resulting in the spinel-like surface transformation (see Fig. 2a). However, in systems with electrolyte, we see additional opportunities for the surface degradation process, with the continuous extraction of oxygen from the surface by the reactions involving electrolyte. Moreover, during the typical cycling process of the battery, these surfaces will be experiencing Li diffusion as well, leading to additional dynamics exposing the surface for attack from electrolyte. Therefore, based on the above results, we propose that there will be a continued evolution of O_2 from the surfaces interacting with the electrolyte compared to a more settled surface as seen in the systems without electrolyte.

We note that the Ni/Li disorder (defect concentration reported to be $2\sim3\%$ for high-Ni NMCs) impacting the electrochemical performance of Ni-rich layered oxides and has been investigated more recently. ⁴⁰ While our current study does not directly assess the effects of this disorder due to the computational scope, we highlight this as an important aspect for future computational investigations.



Charge Analysis of Ni

The individual charge transfers were observed to be minimal and more uniform in the fixed and secondary Ni ions (bulk region) while the Ni ions in the surface exhibited higher variations (Figs. S7 and S8). This was observed concurrently with the formation of O_2 on the surface and due to the interaction with salt ions near the surface. The effect of molecules near the surface or undergoing reactions on the atomic charge of Ni was verified by looking at time-steps where significant variations were observed and then visually co-relating with the movement of the atoms (Sec. 8 in SI).

The Ni ions closer to the surface show a higher deviation in the change in net atomic charges, as calculated using the DDEC6 method (Fig. S10). The DDEC6 method was developed as a net atomic charge (NAC) partitioning method by ensuring each atom has a distinct electron distribution, maintaining core electrons with their atoms, and being independent of the basis set due to total electron density functionality. It supports efficient multipole expansions for precise electrostatic potentials and aligns with electronegativity trends for predictable electron transfers, especially for the lithiation and delithiation of the cathode used in the present work. DDEC6 stood out for its transferability across different molecular conformations, chemical consistency with atomic spin moments, and the scalability of computation of the NACs for this work. Additionally, it addresses issues like non-nuclear attractors and offers broad applicability across material types where the Bader approach has reportedly failed in assigning the atomic charge in some systems. 41,42

The initial drop in the charge value for the Ni ions closer to the surface is a result of the relaxation of the structure with surface ions undergoing a considerable reformation to balance the dangling bonds at the surface, referred to as the surface reconstruction layer (SRL). This variation in the atomic charge of Ni atoms decreases as one goes down the layers. This is attributed to the relatively constrained ion dynamics below the surface layer as well as due to lack of interactions with the electrolyte molecules (in electrolytic systems). We find a mismatch in the results of net atomic charge transfer in Ni calculated from the DDEC6 method compared to the Bader method. We discuss and present our results in Sec. 9 in SI and in Figs.S10-S13. We note that a retraining of the DDEC6 datasets may be necessary to properly account for calculation of net atomic charges in LiNiO₂ systems.

Degradation of electrolyte

Surface electrolyte decomposition facilitated the formation of H_2O , CO_2 , CO_3 ²⁻ and decomposed EC/DMC fragments, which were stable and stayed on the surface. Decomposition products were independent of the salt used. There were no observations of electrolyte molecules reacting with each other or with the $LiPF_6$ or $LiBF_4$ salts in any of the trajectories. We note that the limited time length of the trajectory in the AIMD approach used in this study may have been a contribution to this observation. Some salt ion pairs dissociated from contact-ion pairs into solvent-separated ion pairs, as discussed in our previous work focusing on solvation shells in the electrolyte region; an example is shown in Fig. S17.⁴³ Here, the Li^+ and PF_6^- ions separate on the surface, with Li^+ getting deposited on the surface. Subsequently, the PF_6^- forms a new solvation shell. Other ion pairs dissociated on the surface, resulting in Li^+ deposition as in Fig. S17.

Reaction pathways - Formation of H₂O

Deprotonation of EC and DMC molecules was observed frequently in de-lithiated systems in all four trajectories. The hydrogen atoms stripped from the EC molecule, promptly formed hydroxyls with the surface oxygens. Furthermore, these hydrogen atoms had a tendency to hop across the surface using nearby oxygen atoms. For example, two hydrogens (originally from a dissociated EC molecule) moved across the cathode surface forming an H_2O molecule (Fig. 3) for a very brief period (~350 fs), after which it disintegrated. Experimentally, it is exceedingly difficult to eliminate the hydroxyls from the cathode surface even under high and prolonged thermal exposure (750 $^{\circ}$ C), and leads to the formation of H_2O on cathode surface.⁴⁴

On a subsequent system which started with a hydrogen-terminated cathode surface (50%), H_2O formation was seen to be much more frequent, and prevalence of the molecule was more sustained (~4-6 ps vs. ~0.12 ps). Our observations confirm the experimental observations and provide a secondary source for the creation of H_2O at the cathode interface. Surface degradation pathways, either through formation of molecular oxygen or molecular H_2O , seemed to be dependent on the presence of hydrogen on the delithiated cathode surface. Where heavily passivated, the surface would erode by non-reversible evolution of H_2O . In the absence of passivation, the surface would degrade by formation of molecular O_2 .

The electrochemical role water and other protic sources play in Ni rich batteries is quite significant. The water and the protic species forming at the cathodes have recently been reported to be migratory towards the anode, where they will react with SEI components and contribute to the capacity fade in the overall battery system.^{39,45} Electrochemical reduction of these species can also account for the release of H₂ gas as reported recently by Dose et al. using Online Electrochemical Mass Spectroscopy (OEMS) results.³⁹ More importantly, since the reduction of water has also been reported at low potentials (1.55 V vs Li/Li*) in lithium titanate (LTO) anodes⁴⁶, this effect needs to be considered more carefully for most of the common anodes currently used in batteries.



Reaction pathways - Formation of CO₂

The complete disintegration of EC molecules was infrequent. More often, a singular de-hydrogenation of either EC or DMC molecules was observed. A full decomposition reaction involving an EC molecule, initiated by dehydrogenation of EC, resulting in 3 CO₂ molecules is given in Fig. 4, with the proposed reaction pathway as shown in Fig. S19. After rapid removal of two hydrogen atoms bonded to two adjacent primary carbon atoms in the EC molecule (Fig. 4-A,B), the ring starts to break apart (Fig. 4-C). Fig. 4-D,E shows an instance where the formation of a H₂O and a surface O₂ molecule is observed. The carbonyl carbon breaks away with two of the oxygen atoms in the EC molecule, forming the first CO₂ molecule (Fig. 4-F). A C₂H₂O complex bonding to surface oxygen is then observed (Fig. 4-G). After a considerable period of random swaying, the two carbon atoms acquire extra oxygen atoms from the surface (Fig. 4-H,I) and drift off from the surface, with a total of 3 CO₂ molecules being produced in the decomposition process (Fig. 4-K).

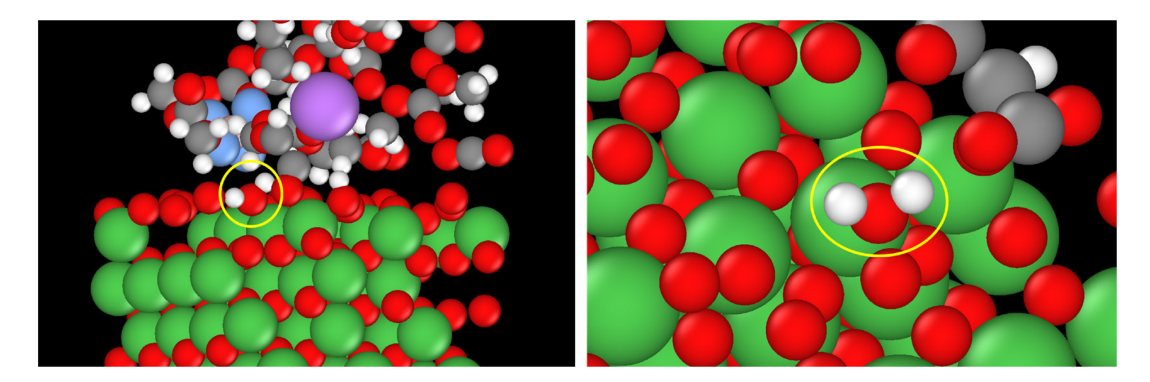


Figure 3. Formation of a temporary H₂O on the surface of the de-lithiated cathode (shown here from different perspectives, across the interface (left), and from the top (right), with and without the presence of electrolyte molecules for clarity). Ni-Green, O-Red, C-Grey, Li-Purple, F-Blue, H-White

In another trajectory, the hydrogens from the EC molecule transfer onto the delithiated cathode surface, initiating a reaction pathway resulting in the formation of CO_3^{2-} species at the interface (see Fig. S20 for the proposed reaction pathway). Interestingly, we observed the participation of a singlet oxygen species at the surface towards the end of the reaction resulting in a bicarbonate at the cathode surface (Fig. S20). This bicarbonate eventually breaks down into a carbonate which is adsorbed to the cathode surface for the rest of the trajectory.

In both of these decomposition pathways, we identified that the two oxygen species at the surface (radical and coordinated oxygens bridging the surface Ni ions) play a pivotal role in initiating a rapid removal of protons from EC. The proposed reaction pathways observed for the EC degradation reactions confirm the nucleophilic attack and dissociation of an EC molecule as proposed by the Yang group. 47,48

Alternative Electrolyte systems

The reactivity of the components in the system was minimal in the initial trajectory time lengths accessible in AIMD. Therefore, a few additional systems were set up to observe the effects of the presence of decomposition products in contact with lithiated cathodes. On an individual basis, additional O₂, H₂O, HF and PF₅+HF were inserted into separate simulation cells.

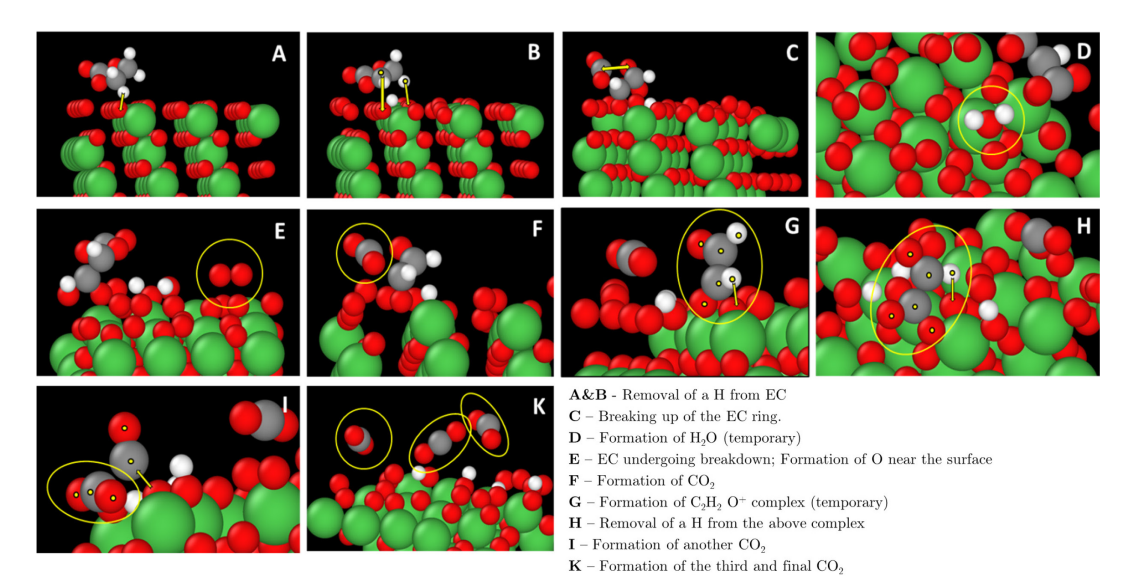


Figure 4. Process of disintegration of an EC molecule upon dehydrogenation leading to the formation of CO_2 molecules. The EC molecule interacts with a radical oxygen at the cathode surface, removing two H atoms in quick succession (A-B). The deprotonated carbon gets drawn to the surface oxygen, opening the EC ring, and releasing a CO_2 molecule (C). The proton hopping action at the surface can form water molecules at the (012) surface (D). A release in molecular O_2 at the surface is shown (E). As the EC fragment continues evolving at the surface, more CO_2 is released (F). This fragment continues to deprotonate (G-H) and the final fragment extracts oxygen from the surface releasing a CO_2 molecule (I), altogether resulting in 3 CO_2 molecules. See Fig. S19 for the proposed pathway for the reaction.

In all the systems where products were inserted, each had three product molecules added, two of them closer to either surface and one in the middle of the electrolyte region. In the systems where alternative electrolyte components were added (O_2 , H_2O , HF and PF₅+HF), the observations are summarized in Fig. 5. Over time, the O_2 molecules descended onto the cathode surface, while the molecule placed in the center of the electrolyte region did not move considerably. There was no notable observation with regards to the inclusion of H_2O molecules. The HF molecules were seen to dissociate on the surface of the lithiated cathode leading to the formation of stable LiF which remained bound to the cathode surface. The HF within the electrolyte region did not undergo any reactions with the electrolyte molecules. There were no further reactions for the rest of the trajectory (\sim 11 ps). When PF₅ and LiF were placed at the lithiated interface, it was seen that the LiF would dissociate by forming PF₆⁻ and stay bound to the Li at the interface.

Further to that, two systems were simulated at elevated temperatures of 750 K and 850 K for lithiated cathodes with no passivation at the cathode surface (as opposed to the nominal 450 K used for all other calculations). As expected, the reactions proceeded at a higher rate from these accelerated trajectories. However, there were no other significant observations with respect to surface interactions. With hydrogen covered surfaces (50% and 100% coverage), it was seen that the H_2O formation on the surface by way of combination of hydrogens was much more frequent compared to the formation of H_2O from the

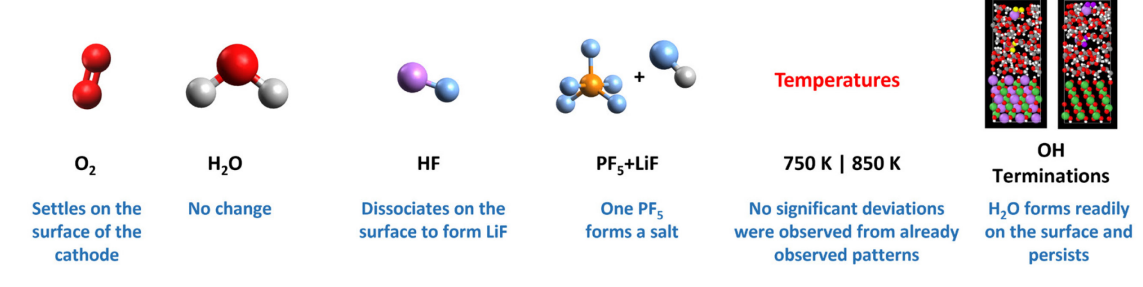


Figure 5: The observations that were noted from the trajectories of alternative systems.



hydrogens obtained from the decomposition of electrolyte molecules. This could have been due to the relatively active nature of the cathode surface with lesser hydrogen terminations relative to half/fully covered cathode surfaces.

For better clarity and benefit of the reader, all notable observations made from the trajectories are summarized in Table 1.

Table 1: Summary of major observations from the trajectories, run at 450 K and with both salts unless specified.

| Details | Cathode Type | Surface | Theory |
|--|-----------------|---------|--------|
| Surface Reactions | | | |
| Formation of O ₂ | NO | NP | Both |
| Desorption of O ₂ | NO | NP | DFT+U |
| EC/DMC dehydrogenation | NO | Both | Both |
| Formation of H ₂ O | NO | Р | Both |
| Carbonate formation | NO | NP | DFT+U |
| CO ₂ formation | NO | NP | Both |
| Cathode Lattice | | | |
| Ni displacement | NO | NP | DFT+U |
| Surface Reconstruction | | | |
| Li protrusion | LNO | NP | Both |
| O ₂ formation | NO | NP | Both |
| Alternate Trajectories (LiBF ₄ salt) | | | |
| Electrolyte | | | |
| Adding O ₂ - No change, free to desorb | LNO | NP | DFT |
| Adding H₂O - No change | LNO | NP | DFT |
| Adding HF - Forms LiF on surface | LNO | NP | DFT |
| Adding LiF+PF ₅ - Forms LiPF ₆ | LNO | NP | DFT |
| Carbonate formation | LNO | NP | DFT |
| Temperature | | | |
| 850/750 K - No deviations | LNO | NP | DFT |
| Vacuum | | | |
| O ₂ formation & desorption | NO | NP | Both |
| Ni Displacement | NO | NP | DFT |

Cathode type: LNO-LiNiO2, NO-NiO2, Surface: P-Passivated, NP-Non passivated

We have carried out detailed atomistic simulations to elucidate the chemical activity of organic electrolytes at Ni-rich cathode surfaces. Our findings highlight the heightened interfacial reactivity of delithiated cathodes. The deprotonation of surface electrolyte occurs irrespective of SOC or surface passivation, albeit at a reduced rate for initially hydrogen passivated surfaces. We observe minimal reactivity at the lithiated cathode interfaces. Notably, the level of passivation at the delithiated cathode surface influences the pathway of surface degradation. In heavily passivated delithiated cathodes, irreversible evolution of H_2O is observed, whereas in non-passivated delithiated cathodes, a non-reversible O_2 evolution takes place. Both lead to the collapse of the lattice resulting in Ni entering the channels which may result in a change from layered to rocksalt-like phase.

We find that the experimentally frequent (012) facet of the Ni-rich cathode surface can contribute to the presence of radical oxygen holes. At highly delithiated states, these exhibit a tendency to combine to form peroxide ions at the surface before migrating into the electrolyte region in the triplet state, transitioning briefly through a singlet state. We also find more reactive radicals initiating and consistently involved in the breakdown of ethylene carbonate, resulting in CO_2 and CO_3^{2-} at the cathode surface, with the latter pathway involving singlet oxygen. The loss of surface oxygen atoms is seen to take place in our trajectories in all the three of the methods described above. However, the spontaneous evolution of O_2 from the initial surface reconstruction is limited to the initial stages whereas the oxygen removal from the surface can happen at any time in the trajectory by way of extraction of oxygen during the degradation of the electrolyte. CO_2 can also evolve from the breakdown of the cyclic EC or the linear DMC molecule (Fig. S19 and S20).



Moreover, the necessity of applying a +U correction in cathode simulations becomes evident as it accurately captures initial stages of TM dissolution/phase change, accounts for the complete desorption of O_2 peroxo species, and indicates increased interface reactivity. Our investigations indicate that the high degree of electron correlation in layered oxides necessitate the use of Hubbard U correction in the first principles based molecular dynamics trajectories to represent the interfacial interactions accurately. The interaction of LiF and PF $_5$ at the interface results in the formation of LiPF $_6$. The presence of HF leads to the formation of stable LiF at the interface. Interestingly, we found no substantial variation in the reactivity of different salts. Furthermore, our charge calculations reveal the reduction of Ni atoms on the cathode surface relative to the bulk cathode.

Surface treatments that utilize controlled passivation levels could be a way to control the initial SEI formation and substantially lower the adverse reactions at the cathode-electrolyte interface, although further investigations are necessary to fully understand the effects of hydrogen passivation across different surfaces and cathode types. Additionally, selecting alternative coatings or additives that interact favorably with the cathode surface and electrolyte can effectively manage interfacial reactions. Suppressing reactive radical formation at the cathode surface provides an additional strategy for minimizing side reactions, enhancing the overall efficiency and safety of lithium-ion batteries. We emphasize the critical role of understanding and controlling the complex interfacial reactivity, and believe this work offers meaningful atomistic insights and motivation for future work involving targeted surface modifications at the electrode and electrolyte interfaces.

EXPERIMENTAL PROCEDURES

Resource Availability

Lead Contact

Further information and requests for resources should be directed to and will be fulfilled by the Lead Contact, Manuel Smeu (msmeu@binghamton.edu).

Data and Code Availability

The code generated during this study is available at the repository: [https://zenodo.org/doi/10.5281/zenodo.11158137]. Extra trajectory data can be requested via email from the Lead Contact, Manuel Smeu (msmeu@binghamton.edu).

Materials Availability

No unique materials were generated in the study.

Computational details

The interaction of the organic electrolyte with Ni-rich cathode was modeled using the Vienna Ab initio Simulation Package (VASP). Projector augmented wave (PAW) potentials were used to mimic the ionic cores 49.51 and the Perdew-Burke-Ernzerhof (PBE) generalized gradient approximation (GGA) provided the exchange and correlation functional 52.53 with a Γ-centered 1×1×1 Monkhorst-Pack k-point grid used for all structural relaxations and energy calculations. The Brillouin zone was sampled using Gaussian smearing.

DFT calculations were performed using a plane wave energy cutoff set at 700 eV. The primitive cells for the cathodes were obtained from the Materials Project repository (MP-25411).⁵⁶ Design and visual analysis of the systems was done using Ovito and Vesta, with Avogadro being used to create the initial electrolyte configurations.^{57–59}

Four distinct systems: lithiated and delithiated, with LiBF $_4$ or LiPF $_6$ as the salt, were used to model the interactions. Systems without an electrolyte component were used as references (Fig. 1). The AIMD simulations were run at 450 K with 1-fs time steps using the canonical (NVT) ensemble simulating the system at open-circuit voltage (OCV). Our systems represent fully discharged and highly charged cathode surfaces by way of the degree of lithiation at the cathode interface at the open circuit state. DFT allows for the localized electron transfer at the cathode-electrolyte interface in either direction based on local potential variations. All the AIMD calculations were performed with a plane wave energy cutoff set at 400 eV using a Γ -centered k-point. A separate set of AIMD calculations were run with Hubbard U correction (GGA+U) that accounts for the delocalization of 3U0 electron states of Ni. And U1 der Waals interactions were included via the Grimme D3 approach (PBE-D3) with Becke-Johnson damping in all calculations.

Each system was simulated for a minimum duration of 10 ps, utilizing a timestep of 1 fs. In cases where distinct reactions (molecule degradation, surface interactions) were detected in a system, the trajectory length was extended to facilitate the observation of either reaction pathway's endpoints or the formation of stable products. Moreover, four additional trajectories were run, mirroring the composition of the four primary cathode systems (Fig. 1) but exhibiting altered initial configurations in the electrolyte region for improved statistics. These trajectories underwent testing up to a temperature of 750 K during the design phase, while comparable systems have been examined at temperatures up to 800 K in recent studies. 11,65–67 This methodology is frequently employed to accelerate reactions and equilibrate more rapidly in AIMD simulations. For our production runs, we implemented a temperature control at 450 K in our investigation, to ensure the chemical stability of the studied system and to secure a practical trajectory window for the simulation timescales. More importantly, the electrolyte systems remained chemically stable, showing no anomalous effects due to temperature regulation.



The equilibration of the systems is critical in MD simulations and was verified by monitoring energy changes for a given system with time. Additionally, the regulation of the temperature, electronic convergence and consistent convergence of the spin states (for DFT+*U* trajectories) of the calculation was closely monitored.

Charge analysis was primarily performed using the refined density-derived electrostatic and chemical (DDEC6) approach⁶⁸ as implemented in the Chargemol code, ⁶⁹ while the Bader method was used to verify the results initially. ^{68,70} Analysis of the trajectories, including but not limited to the observations of reactions, decomposition of molecules, interatomic distances, visualization of the change in charge and spin, etc., were done using the cluster analysis and color-coding options in the Ovito program. ⁵⁷ The electron localization function (ELF) is computed as implemented in VASP and ELF isosurfaces were visualized using Vesta. ⁵⁸ Bond distances were calculated using a python script developed in-house. The results were initially cross-checked with the Ovito software to ascertain the accuracy.

Design of Systems for AIMD

There are a number of systems that have been investigated as a part of this study. Overall, there are four main distinct systems that vary on the degree of lithiation and the type of salt in the electrolyte (Fig. 1). Four more systems were created which are equal to the former but with different starting configurations in the electrolyte region for improved statistics. Two systems (lithiated and delithiated) with the electrolyte region replaced with vacuum were used as reference systems. Another set of systems were modeled with the cathode surface 50% passivated using hydrogen terminations. We investigate the role played by the Hubbard *U* correction in the AIMD simulations of transition metal oxides by running the original four systems with the *U* correction applied. We also simulate the effects of decomposition products on cathode surface in a few specific systems.

Cathodes

The cathodes were designed such that they represent a layered fully lithiated (fully discharged) LiNiO₂ (LNO) or a fully delithiated (fully charged) NiO₂ (NO) state (Fig. 1). The (012) plane is used at the electrolyte-cathode interface, ensuring the periodicity of the cathode in two directions. The (012) plane was chosen as it served as an active and stable interface for the cathode-electrolyte.⁷¹ The impact of passivation was examined employing slab surfaces passivated by hydrogen terminations, which accounted for 50% of the cathode surface (Fig. S1). This was part of the alternate systems used for further investigations.

Our work uses periodic systems across boundaries as typically used in plane wave DFT calculations. We leverage the periodic nature of the VASP simulation cells to model two electrolyte-cathode interfaces in a single simulation as repetitive alternate layers of cathode and electrolyte. Therefore, the slabs were initially prepared from a fully structurally relaxed bulk system. The lithiated and delithiated systems were prepared from separately relaxed bulk systems. The slab was then prepared as shown on Fig. S5. The atoms in the middle layer ('Bulk') were constrained in all directions to simulate the bulk region of the cathode, while all other atoms were unconstrained to simulate the dynamical nature of the interface. Our observations are made from both sides of the cathode which were quite uniform and consistent on all trajectories. This approach is consistent with other studies in literature that employ similar models without vacuum regions. ^{11,66,67,72} The planar averaged local potential for these systems illustrates that the potential is periodic within the cathode region, changes smoothly and continuously into the electrolyte region and maintains a consistent profile within the electrolyte (Fig. S21).

The Hubbard U value we used was derived from literature on investigations into similar systems, both in bulk and slab systems. The values typically used in similar work range from 6.04 - 6.7 eV specifically to account for their various oxidation states of Ni and oxidation energies within the LDA and GGA frameworks. 63,73 More specifically, we used the average of the two studies in our work (6.2 eV). 73,74

Due to the surface atoms having a lower coordination number, the localization of electrons on the surface would be lower than those in the bulk. Indeed, it has recently been reported that the U value of surface atoms to be smaller than the bulk optimized U value to address the lesser degree of electron delocalization on the TMO surfaces, specifically NiO. Therefore, it may be more appropriate in future work to consider optimizing the U parameter for bulk and surface Ni atoms separately.

For ease of charge analysis, the Ni ions were classified into three distinct layers, namely, the 'surface layer' which is exposed to the electrolyte/vacuum, the 'secondary layer' which is immediately below the surface layer and the 'fixed layer' which was constrained to simulate the bulk of the cathode (Fig. S5). In the charge calculations, the cathodes combined with the electrolyte will be identified as 'electrolyte cathodes' and the systems without any electrolyte present will be identified as 'bare/vacuum cathodes' (a vacuum replaces the volume of electrolyte).

Electrolytes

LiBF $_4$ and LiPF $_6$ salts were placed in the electrolyte regions to investigate if there is a salt dependent effect on the cathode-electrolyte interface and to observe the possible processes within the electrolyte. Table S1 in the SI summarizes the species and the number of atoms used in building up the electrolyte system. In all the systems, 14 pairs of EC and DMC molecules were placed randomly. LiPF $_6$ or LiBF $_4$ salt pairs were also added, with one closer to the cathode surface, another near the middle of the electrolyte volume. This was to observe interactions readily within the limited time available for calculations while ensuring that such placement did not result in biased or unrealistic observations.



We utilized a top-down method to ascertain the system volume, where a commercially available experimental concentration of 1M EC/DMC was aligned with the molecular concentration in our simulation cells. The requisite number of molecules to reach this concentration was randomly placed within the cell. Following this, the system underwent relaxation via DFT prior to its positioning adjacent to the cathode. We incorporated van der Waals distances for oxygen on both sides of the cell to counteract Coulombic repulsion. Consequently, this led to an electrolyte region with an approximate density of 1.28 g·cm⁻³.

Although our calculations are inspired by high energy density Ni-rich NMC, modeling such minute concentrations of Mn and Co is currently unfeasible due to cathode size constraints within DFT. Therefore, we have chosen $LiNiO_2$ to exemplify an end member of NMC-type oxides. Additionally, to discern reactions taking place at varying battery charge stages, we also examine fully delithiated NiO_2 .

SUPPLEMENTAL INFORMATION

All data needed to evaluate the conclusions in the study are presented in the paper or supplemental information.

ACKNOWLEDGMENTS

This work was supported by the National Science Foundation under Grant No. CBET-2028722. This work was performed using Expanse, a part of the Extreme Science and Engineering Discovery Environment (XSEDE), which is supported by National Science Foundation Grant No. 1928224 under allocation TG-DMR180009 and Spiedie HPC at Binghamton University.

AUTHOR CONTRIBUTIONS

M.D. Hashan C. Peiris: Validation, Formal analysis, Data curation, Writing – original draft, Writing – review & editing. **Diana Liepinya**: Investigation, Writing – review & editing. **Hao Liu**: Supervision, Writing – review & editing, Funding acquisition. **Manuel Smeu**: Conceptualization, Writing – review & editing, Supervision, Project administration, Funding acquisition.

DECLARATION OF INTERESTS

The authors declare no competing interests.



REFERENCES

- 1. Laure Monconduit, Rémi Dedryvère, and Laurence Croguennec (2015). Electrodes for Li-ion Batteries (Wiley).
- 2. Xu, K. (2014). Electrolytes and Interphases in Li-Ion Batteries and Beyond. Chem. Rev. 114, 11503–11618. 10.1021/cr500003w.
- 3. Jiang, Y., Yan, P., Yu, M., Li, J., Jiao, H., Zhou, B., and Sui, M. (2020). Atomistic mechanism of cracking degradation at twin boundary of LiCoO2. Nano Energy 78, 105364. 10.1016/j.nanoen.2020.105364.
- 4. Kaur, G., and Gates, B.D. (2022). Review—Surface Coatings for Cathodes in Lithium Ion Batteries: From Crystal Structures to Electrochemical Performance. J. Electrochem. Soc. *169*, 043504. 10.1149/1945-7111/ac60f3.
- 5. Manthiram, A., and Goodenough, J.B. (1987). Lithium insertion into Fe2(MO4)3 frameworks: Comparison of M = W with M = Mo. Journal of Solid State Chemistry 71, 349–360. 10.1016/0022-4596(87)90242-8.
- Manthiram, A., and Goodenough, J.B. (1989). Lithium insertion into Fe2(SO4)3 frameworks. Journal of Power Sources 26, 403–408. 10.1016/0378-7753(89)80153-3.
- Bianchini, M., Roca-Ayats, M., Hartmann, P., Brezesinski, T., and Janek, J. (2019). There and Back Again—The Journey of LiNiO ₂ as a Cathode Active Material. Angew. Chem. Int. Ed. 58, 10434–10458. 10.1002/anie.201812472.
- 8. Ge, J., Xie, M., Zhao, Q., Zhang, S., and Sun, H. (2023). Advances in Co-free layered cathode materials for Li-ion batteries. International Journal of Electrochemical Science 18, 100292. 10.1016/j.ijoes.2023.100292.
- 9. Zheng, J., Ye, Y., Liu, T., Xiao, Y., Wang, C., Wang, F., and Pan, F. (2019). Ni/Li Disordering in Layered Transition Metal Oxide: Electrochemical Impact, Origin, and Control. Acc. Chem. Res. 52, 2201–2209. 10.1021/acs.accounts.9b00033.
- 10. Rougier, A., Delmas, C., and Chadwick, A.V. (1995). Non-cooperative Jahn-Teller effect in LiNiO2: An EXAFS study. Solid State Communications 94, 123–127. 10.1016/0038-1098(95)00020-8.
- 11. Young, J., Kulick, P.M., Juran, T.R., and Smeu, M. (2019). Comparative Study of Ethylene Carbonate-Based Electrolyte Decomposition at Li, Ca, and Al Anode Interfaces. ACS Appl. Energy Mater. 2, 1676–1684. 10.1021/acsaem.8b01707.
- 12. Lide M. Rodriguez-Martinez and Noshin Omar (2017). Emerging nanotechnologies in rechargeable energy storage systems Lide M. Rodriguez-Martinez, ed. (Elsevier Inc.).
- 13. Hu, L., Zhang, Z., and Amine, K. (2013). Electrochemical investigation of carbonate-based electrolytes for high voltage lithium-ion cells. Journal of Power Sources 236, 175–180. 10.1016/J.JPOWSOUR.2013.02.064.
- 14. Jow, T.R., Xu, K., Borodin, O., and Ue, M. eds. (2014). Electrolytes for Lithium and Lithium-Ion Batteries 2014th edition. (Springer).
- 15. Edge, J.S., O'Kane, S., Prosser, R., Kirkaldy, N.D., Patel, A.N., Hales, A., Ghosh, A., Ai, W., Chen, J., Yang, J., et al. (2021). Lithium ion battery degradation: what you need to know. Physical Chemistry Chemical Physics 23, 8200–8221. 10.1039/D1CP00359C.
- 16. Xu, C., Märker, K., Lee, J., Mahadevegowda, A., Reeves, P.J., Day, S.J., Groh, M.F., Emge, S.P., Ducati, C., Layla Mehdi, B., et al. (2021). Bulk fatigue induced by surface reconstruction in layered Ni-rich cathodes for Li-ion batteries. Nat. Mater. 20, 84–92. 10.1038/s41563-020-0767-8.
- 17. Gao, Y., Wang, Z., and Chen, L. (2015). Workfunction, a new viewpoint to understand the electrolyte/electrode interface reaction. J. Mater. Chem. A 3, 23420–23425. 10.1039/C5TA07030A.
- 18. Xu, K. (2004). Nonaqueous Liquid Electrolytes for Lithium-Based Rechargeable Batteries. Chem. Rev. 104, 4303–4418. 10.1021/cr030203g.
- 19. Xu, K. (2021). Li-ion battery electrolytes. Nat Energy 6, 763-763. 10.1038/s41560-021-00841-6.
- 20. Manthiram, A. (2020). A reflection on lithium-ion battery cathode chemistry. Nat Commun *11*, 1550. 10.1038/s41467-020-15355-0.
- 21. Liu, T., Liu, J., Li, L., Yu, L., Diao, J., Zhou, T., Li, S., Dai, A., Zhao, W., Xu, S., et al. (2022). Origin of structural degradation in Li-rich layered oxide cathode. Nature *606*, 305–312. 10.1038/s41586-022-04689-y.
- 22. Li, Q., Chen, J., Fan, L., Kong, X., and Lu, Y. (2016). Progress in electrolytes for rechargeable Li-based batteries and beyond. Green Energy and Environment 1, 18–42. 10.1016/j.gee.2016.04.006.
- 23. Genreith-Schriever, A.R., Banerjee, H., Menon, A.S., Bassey, E.N., Piper, L.F.J., Grey, C.P., and Morris, A.J. (2023). Oxygen hole formation controls stability in LiNiO2 cathodes. Joule 7, 1623–1640. 10.1016/j.joule.2023.06.017.
- 24. Freiberg, A.T.S., Roos, M.K., Wandt, J., De Vivie-Riedle, R., and Gasteiger, H.A. (2018). Singlet Oxygen Reactivity with Carbonate Solvents Used for Li-Ion Battery Electrolytes. J. Phys. Chem. A *122*, 8828–8839. 10.1021/acs.jpca.8b08079.
- 25. Rinkel, B.L.D., Vivek, J.P., Garcia-Araez, N., and Grey, C.P. (2022). Two electrolyte decomposition pathways at nickel-rich cathode surfaces in lithium-ion batteries. Energy Environ. Sci. 15, 3416–3438. 10.1039/D1EE04053G.



- 26. Jung, R., Metzger, M., Maglia, F., Stinner, C., and Gasteiger, H.A. (2017). Oxygen Release and Its Effect on the Cycling Stability of LiNi x Mn y Co z O 2 (NMC) Cathode Materials for Li-Ion Batteries. J. Electrochem. Soc. 164, A1361–A1377. 10.1149/2.0021707jes.
- 27. Mullinax, J.W., Bauschlicher, C.W., and Lawson, J.W. (2021). Reaction of Singlet Oxygen with the Ethylene Group: Implications for Electrolyte Stability in Li-Ion and Li-O ₂ Batteries. J. Phys. Chem. A *125*, 2876–2884. 10.1021/acs.jpca.1c00605.
- 28. Wandt, J., Freiberg, A.T.S., Ogrodnik, A., and Gasteiger, H.A. (2018). Singlet oxygen evolution from layered transition metal oxide cathode materials and its implications for lithium-ion batteries. Materials Today *21*, 825–833. 10.1016/j.mattod.2018.03.037.
- 29. Das, H., Urban, A., Huang, W., and Ceder, G. (2017). First-Principles Simulation of the (Li–Ni–Vacancy)O Phase Diagram and Its Relevance for the Surface Phases in Ni-Rich Li-Ion Cathode Materials. Chem. Mater. 29, 7840–7851. 10.1021/acs.chemmater.7b02546.
- 30. Gu, X., Liu, J., Yang, J., Xiang, H., Gong, X., and Xia, Y. (2011). First-Principles Study of H ⁺ Intercalation in Layer-Structured LiCoO ₂. J. Phys. Chem. C *115*, 12672–12676. 10.1021/jp202846p.
- 31. Benedek, R., Thackeray, M.M., and Van De Walle, A. (2008). Free Energy for Protonation Reaction in Lithium-lon Battery Cathode Materials. Chem. Mater. 20, 5485–5490. 10.1021/cm703042r.
- 32. Choi, J., Alvarez, E., Arunkumar, T.A., and Manthiram, A. (2006). Proton Insertion into Oxide Cathodes during Chemical Delithiation. Electrochem. Solid-State Lett. 9, A241. 10.1149/1.2184495.
- 33. Kong, F., Liang, C., Wang, L., Zheng, Y., Perananthan, S., Longo, R.C., Ferraris, J.P., Kim, M., and Cho, K. (2019). Kinetic Stability of Bulk LiNiO 2 and Surface Degradation by Oxygen Evolution in LiNiO 2 -Based Cathode Materials. Advanced Energy Materials 9, 1802586. 10.1002/aenm.201802586.
- 34. Garcia, J.C., Bareño, J., Yan, J., Chen, G., Hauser, A., Croy, J.R., and Iddir, H. (2017). Surface Structure, Morphology, and Stability of Li(Ni 1/3 Mn 1/3 Co 1/3)O 2 Cathode Material. J. Phys. Chem. C 121, 8290–8299. 10.1021/acs.jpcc.7b00896.
- 35. Nurdin, L., Spasyuk, D.M., Fairburn, L., Piers, W.E., and Maron, L. (2018). Oxygen–Oxygen Bond Cleavage and Formation in Co(II)-Mediated Stoichiometric O 2 Reduction via the Potential Intermediacy of a Co(IV) Oxyl Radical. J. Am. Chem. Soc. 140, 16094–16105. 10.1021/jacs.8b07726.
- 36. Silvi, B., and Savin, A. (1994). Classification of chemical bonds based on topological analysis of electron localization functions. Nature *371*, 683–686. 10.1038/371683a0.
- Schweitzer, C., and Schmidt, R. (2003). Physical Mechanisms of Generation and Deactivation of Singlet Oxygen. Chem. Rev. 103, 1685–1758. 10.1021/cr010371d.
- 38.E. Spotte-Smith, Sudarshan Vijay, Thea Bee Petrocelli, Bernardine L. D. Rinkel, Bryan D. McCloskey, and Kristin A. Persson (2024). A Critical Analysis of Chemical and Electrochemical Oxidation Mechanisms in Li-Ion Batteries. Journal of Physical Chemistry Letters. 10.1021/acs.jpclett.3c03279.
- 39. Dose, W.M., Temprano, I., Allen, J.P., Björklund, E., O'Keefe, C.A., Li, W., Mehdi, B.L., Weatherup, R.S., De Volder, M.F.L., and Grey, C.P. (2022). Electrolyte Reactivity at the Charged Ni-Rich Cathode Interface and Degradation in Li-Ion Batteries. ACS Appl. Mater. Interfaces 14, 13206–13222. 10.1021/acsami.1c22812.
- 40. Yin, L., Li, Z., Mattei, G.S., Zheng, J., Zhao, W., Omenya, F., Fang, C., Li, W., Li, J., Xie, Q., et al. (2020). Thermodynamics of Antisite Defects in Layered NMC Cathodes: Systematic Insights from High-Precision Powder Diffraction Analyses. Chem. Mater. 32, 1002–1010. 10.1021/acs.chemmater.9b03646.
- 41. Manz, T.A., and Limas, N.G. (2016). Introducing DDEC6 atomic population analysis: part 1. Charge partitioning theory and methodology. RSC Advances 6, 47771–47801. 10.1039/C6RA04656H.
- 42. Limas, N.G., and Manz, T.A. (2016). Introducing DDEC6 atomic population analysis: part 2. Computed results for a wide range of periodic and nonperiodic materials. RSC Adv. 6, 45727–45747. 10.1039/C6RA05507A.
- 43. Peiris, M.D.H.C., Brennan, S., Liepinya, D., Liu, H., and Smeu, M. (2023). Computational determination of the solvation structure of LiBF4 and LiPF6 salts in battery electrolytes. Colloids and Surfaces A: Physicochemical and Engineering Aspects, 131831. 10.1016/j.colsurfa.2023.131831.
- 44. Moses, A.W., Flores, H.G.G., Kim, J.G., and Langell, M.A. (2007). Surface properties of LiCoO2, LiNiO2 and LiNi1-xCoxO2. Applied Surface Science 253, 4782–4791. 10.1016/J.APSUSC.2006.10.044.
- 45. Heiskanen, S.K., Laszczynski, N., and Lucht, B.L. (2020). Perspective—Surface Reactions of Electrolyte with LiNi x Co y Mn z O 2 Cathodes for Lithium Ion Batteries. J. Electrochem. Soc. 167, 100519. 10.1149/1945-7111/ab981c.
- 46. Bernhard, R., Meini, S., and Gasteiger, H.A. (2014). On-Line Electrochemical Mass Spectrometry Investigations on the Gassing Behavior of Li ₄ Ti ₅ O ₁₂ Electrodes and Its Origins. J. Electrochem. Soc. *161*, A497–A505. 10.1149/2.013404ies.
- 47. Gauthier, M., Carney, T.J., Grimaud, A., Giordano, L., Pour, N., Chang, H.-H., Fenning, D.P., Lux, S.F., Paschos, O., Bauer, C., et al. (2015). Electrode–Electrolyte Interface in Li-lon Batteries: Current Understanding and New Insights. J. Phys. Chem. Lett. 6, 4653–4672. 10.1021/acs.jpclett.5b01727.



- 48. Giordano, L., Karayaylali, P., Yu, Y., Katayama, Y., Maglia, F., Lux, S., and Shao-Horn, Y. (2017). Chemical Reactivity Descriptor for the Oxide-Electrolyte Interface in Li-Ion Batteries. J. Phys. Chem. Lett. 8, 3881–3887. 10.1021/acs.jpclett.7b01655.
- 49. Kresse, G., and Hafner, J. (1994). Norm-conserving and ultrasoft pseudopotentials for first-row and transition elements. Journal of Physics: Condensed Matter 6, 8245. 10.1088/0953-8984/6/40/015.
- 50. Kresse, G., and Furthmüller, J. (1996). Efficiency of ab-initio total energy calculations for metals and semiconductors using a plane-wave basis set. Computational Materials Science 6, 15–50. 10.1016/0927-0256(96)00008-0.
- 51. Kresse, G., and Joubert, D. (1999). From ultrasoft pseudopotentials to the projector augmented-wave method. Physical Review B Condensed Matter and Materials Physics *59*, 1758–1775. 10.1103/PhysRevB.59.1758.
- 52. Perdew, J.P., Burke, K., and Ernzerhof, M. (1996). Generalized Gradient Approximation Made Simple. Physical Review Letters 77, 3865. 10.1103/PhysRevLett.77.3865.
- 53. Perdew, J.P., Burke, K., and Ernzerhof, M. (1997). Generalized Gradient Approximation Made Simple [Phys. Rev. Lett. 77, 3865 (1996)]. Physical Review Letters 78, 1396. 10.1103/PhysRevLett.78.1396.
- 54. Monkhorst, H.J., and Pack, J.D. (1976). Special points for Brillouin-zone integrations. Phys. Rev. B 13, 5188–5192. 10.1103/PhysRevB.13.5188.
- 55. Pack, J.D., and Monkhorst, H.J. (1977). "Special points for Brillouin-zone integrations"---a reply. Phys. Rev. B *16*, 1748–1749. 10.1103/PhysRevB.16.1748.
- 56. Jain, A., Ong, S.P., Hautier, G., Chen, W., Richards, W.D., Dacek, S., Cholia, S., Gunter, D., Skinner, D., Ceder, G., et al. (2013). Commentary: The Materials Project: A materials genome approach to accelerating materials innovation. APL Materials *1*, 011002. 10.1063/1.4812323.
- 57. Stukowski, A. (2009). Visualization and analysis of atomistic simulation data with OVITO-the Open Visualization Tool. Modelling and Simulation in Materials Science and Engineering 18, 015012. 10.1088/0965-0393/18/1/015012.
- 58. Momma, K., and Izumi, F. (2011). VESTA 3 for three-dimensional visualization of crystal, volumetric and morphology data. Journal of Applied Crystallography 44, 1272–1276. 10.1107/S0021889811038970.
- 59. Hanwell, M.D., Curtis, D.E., Lonie, D.C., Vandermeerschd, T., Zurek, E., and Hutchison, G.R. (2012). Avogadro: An advanced semantic chemical editor, visualization, and analysis platform. Journal of Cheminformatics *4*, 1–17. 10.1186/1758-2946-4-17/FIGURES/14.
- 60. Lee, J.G. (2017). Computational materials science: an introduction Second edition. (CRC Press, Taylor & Francis Group, CRC Press is an imprint or the Taylor & Francis Group, an informa business).
- 61.Tolba, S.A., Gameel, K.M., Ali, B.A., Almossalami, H.A., and Allam, N.K. (2018). The DFT+U: Approaches, Accuracy, and Applications. In Density Functional Calculations Recent Progresses of Theory and Application, G. Yang, ed. (InTech). 10.5772/intechopen.72020.
- 62. Shepard, R., Brennan, S., Juran, T.R., Young, J., and Smeu, M. (2022). Ab initio determination of a simultaneous dual-ion charging mechanism for Ni0.25Mn0.75O2 through redox reactions of Ni2+/Ni4+ and O2-/O-. J. Mater. Chem. A 10, 18916–18927. 10.1039/D2TA03938A.
- 63. Zhou, F., Cococcioni, M., Marianetti, C.A., Morgan, D., and Ceder, G. (2004). First-principles prediction of redox potentials in transition-metal compounds with \$\mathrm{LDA}+U\$. Phys. Rev. B 70, 235121. 10.1103/PhysRevB.70.235121.
- 64. Grimme, S., Antony, J., Ehrlich, S., and Krieg, H. (2010). A consistent and accurate ab initio parametrization of density functional dispersion correction (DFT-D) for the 94 elements H-Pu. The Journal of Chemical Physics *132*, 154104. 10.1063/1.3382344.
- 65. Leung, K. (2012). First-principles modeling of the initial stages of organic solvent decomposition on Li xMn 20 4(100) surfaces. Journal of Physical Chemistry C *116*, 9852–9861. 10.1021/jp212415x.
- 66.Zhang, B., Lin, Z., Chen, H., Wang, L.-W., and Pan, F. (2020). The stability and reaction mechanism of a LiF/electrolyte interface: insight from density functional theory. J. Mater. Chem. A 8, 2613–2617. 10.1039/C9TA10170E.
- 67. Young, J., and Smeu, M. (2021). Preventing Electrolyte Decomposition on a Ca Metal Electrode Interface Using an Artificial Solid-Electrolyte Interphase. Adv. Theory Simul. *4*, 2100018. 10.1002/adts.202100018.
- 68. Manz, T.A., and Sholl, D.S. (2012). Improved atoms-in-molecule charge partitioning functional for simultaneously reproducing the electrostatic potential and chemical states in periodic and nonperiodic materials. Journal of Chemical Theory and Computation 8, 2844–2867. 10.1021/CT3002199/SUPPL FILE/CT3002199 SI 002.ZIP.
- 69. Manz, T.A. (2017). Program Computing DDEC Atomic Charges. Chargemol (Version: 09_26_2017) [Source code]. https://sourceforge.net/projects/ddec/files/.
- 70. Bader, R.F.W., and Bader, R.F. (1990). Atoms in molecules: a quantum theory (Clarendon Press).



- 71. Kang, J., and Han, B. (2015). First-Principles Study on the Thermal Stability of LiNiO ₂ Materials Coated by Amorphous Al ₂ O ₃ with Atomic Layer Thickness. ACS Appl. Mater. Interfaces 7, 11599–11603. 10.1021/acsami.5b02572.
- 72. Le, J., Iannuzzi, M., Cuesta, A., and Cheng, J. (2017). Determining Potentials of Zero Charge of Metal Electrodes versus the Standard Hydrogen Electrode from Density-Functional-Theory-Based Molecular Dynamics. Phys. Rev. Lett. 119, 016801. 10.1103/PhysRevLett.119.016801.
- 73. Wang, L., Maxisch, T., and Ceder, G. (2006). Oxidation energies of transition metal oxides within the GGA + U framework. Phys. Rev. B 73, 195107. 10.1103/PhysRevB.73.195107.
- 74. Jain, A., Hautier, G., Ong, S.P., Moore, C.J., Fischer, C.C., Persson, K.A., and Ceder, G. (2011). Formation enthalpies by mixing GGA and GGA + U calculations. Phys. Rev. B *84*, 045115. 10.1103/PhysRevB.84.045115.
- 75. Jiang, S., and Mushrif, S.H. (2023). Determining surface-specific Hubbard- *U* corrections and identifying key adsorbates on nickel and cobalt oxide catalyst surfaces. Phys. Chem. Chem. Phys. *25*, 8903–8912. 10.1039/D2CP04814K.





Figure titles and legends

Figure 1

Title: Major systems considered in the study.

The four distinct systems with lithiated and de-lithiated Ni-rich cathodes with LiBF₄ and LiPF₆ as salts in the electrolyte and the vacuum cathodes.

Legend:

fully lithiated (left)

fully delithiated (right)).

Purple-Li, Green-Ni, Red-Oxygen, White-Hydrogen, Grey-Carbon, Orange-P, Pink-Boron, Blue-Fluorine

Figure 2

Title: Evolution of the main cathode-electrolyte systems at the end of the trajectory

(A) Evolution of the cathode surface for non-passivated lithiated (i-ii) and delithiated (iii-iv) surfaces with and without electrolyte, resulting in a surface reconstruction and O_2 evolution in delithiated cathodes (DFT+U). The sustained heights for O_2 molecules evolving at the cathode surface seen in a(iii) is \sim 3.5 Å.

(B) Desorption energies for the surface evolution of an O₂ molecule in a delithiated NiO₂ vacuum cathode, evaluated every 500 fs steps with the variation of the distance between the two neighboring individual oxygen atoms (O1-O2), and the respective Ni neighbors in the process (Ni1-O1 and Ni2-O2). The point in time where the O₂ molecule fully evolves from the surface is indicated by the dashed line, resulting in a slight increase in Ni-Ni separation at the site.

Legend:

Ni-grey, Li-green, O-red, H-white, F-blue, and B contained within the tetrahedrals of F (BF₄⁻).

Figure 3

Title: Formation of a temporary H2O on the surface of the de-lithiated cathode

(shown here from different perspectives, across the interface (left), and from the top (right), with and without the presence of electrolyte molecules for clarity).

Leaend:

Ni-Green, O-Red, C-Grey, Li-Purple, F-Blue, H-White

Figure 4

Title: Process of disintegration of an EC molecule upon dehydrogenation leading to the formation of CO₂ molecules.

The EC molecule interacts with a radical oxygen at the cathode surface, removing two H atoms in quick succession (A-B).

The deprotonated carbon gets drawn to the surface oxygen, opening the EC ring, and releasing a CO₂ molecule (C).

The proton hopping action at the surface can form water molecules at the (012) surface (D).

A release in molecular O₂ at the surface is shown (E).

As the EC fragment continues evolving at the surface, more CO₂ is released (F).

This fragment continues to deprotonate (G-H) and the final fragment extracts oxygen from the surface releasing a CO₂ molecule (I), altogether resulting in 3 CO₂ molecules.

See Fig. S19 for the proposed pathway for the reaction.

Legend: As indicated in Figure 3.

Figure 5

Title: The observations that were noted from the trajectories of alternative systems.





Tables and table titles and legends Table 1

Title: Summary of major observations from the trajectories, run at 450 K and with both salts unless specified.

Legend (for table):

Cathode type: LNO-LiNiO2, NO-NiO2, Surface: P-Passivated, NP-Non passivated

Supplemental information

Document SI. Figures S1–S21 and Table S1